EFFECT ON WAKE FLOW OF ABRUPT ALTERATIONS IN ELLIPTICITY OF AN ORBITING CYLINDER

L. Baranyi
Department of Fluid and Heat Engineering, University of Miskolc, Miskolc, Hungary

ABSTRACT

A finite difference solution is presented for 2D laminar unsteady flow around a circular cylinder in orbital motion placed in a uniform flow in the Reynolds number domain of Re=120-180. Abrupt jumps between two state curves were found in the time-mean and root-mean-square values of the force coefficients under lock-in conditions. This study focuses upon the effect of abrupt alteration of transverse amplitude during computation. It was found that the solution tended to remain in the same state curve after amplitude alteration, inhibiting jumps between states.

1. INTRODUCTION

The near-wake structure of bluff bodies is very rich in complex phenomena. This is true even of a stationary cylinder in uniform flow, accounting for the huge number of studies of stationary cylinders over the years. The situation becomes even more complex when cylinder motion is added. The largest number of studies of cylinder motion have looked at transverse oscillation (among others, Lu and Dalton, 1996; Blackburn and Henderson, 1999). In an experimental study Williamson and Roshko (1988) prepared a wake mode map for transversely oscillating cylinders, showing different vortex shedding domains. Leontini et al. (2006) investigated the wake modes and energy transfer between the cylinder and fluid numerically. Both studies report sudden changes in vortex structure.

Fewer studies are available for in-line cylinder oscillation (e.g. Mureithi and Rodriguez, 2006; Al-Mdallal et al., 2007), and still fewer for the combination of transverse and in-line motion that leads to a cylinder tracing an orbital path. Blevins (1990) points out that tubes in heat exchangers generally vibrate in oval orbits and these orbits vary in shape from nearly straight lines to circles. As the tubes whirl in their orbits, they extract energy from the flow and this, in part, induces instability. This might also occur when a cylinder moves in waves, for instance.

Cylinders orbiting in a uniform flow are still a relatively unexplored topic, although there are studies of fixed cylinders in orbital flow (e.g. Sarpkaya, 1986) or orbiting cylinders in fluid at rest (e.g. Teshauer et al., 2002). Didier and Borges (2006) looked at an orbiting cylinder, in a fully circular orbit alone, versus cylinder oscillation frequency. However, there are no other studies, according to the best knowledge of the author, that investigate the effect of ellipticity on the forces acting on an orbiting cylinder in uniform flow.

When a cylinder orbits in a uniform flow at low Reynolds number, its flow structure changes abruptly at certain values of orbital ellipticity. There appear to be two states between which the solution switches (Baranyi 2004, 2006, 2008). From the data obtained so far, it seems likely that the "basins of attraction" of multiple solutions of this non-linear system have two attractors, in the form of two stable limit cycles.

The two state curves can be reached in different ways: by using different ellipticity values (Baranyi 2004), by changing the initial position of the cylinder (Baranyi 2006, 2008), by flipping the solutions (Baranyi 2007), or by altering the ellipticity in the course of computation, either abruptly or gradually. This paper focuses upon the effect of abrupt ellipticity alteration during computation in order to collect more evidence on what triggers a change from one state to the other.

2. GOVERNING EQUATIONS AND NUMERICAL METHOD

The dimensionless governing equations for an incompressible constant property Newtonian fluid flow around an orbiting circular cylinder are the two components of the Navier-Stokes equations, the continuity equation and pressure Poisson equation written in a non-inertial system fixed to the cylinder:

$$\frac{\partial u}{\partial t}+u\frac{\partial u}{\partial x}+v\frac{\partial u}{\partial y}=-\frac{\partial p}{\partial x}+\frac{1}{\mathrm{Re}}\nabla^2 u-a_{0x}, \qquad (1)$$

$$\frac{\partial v}{\partial t}+u\frac{\partial v}{\partial x}+v\frac{\partial v}{\partial y}=-\frac{\partial p}{\partial y}+\frac{1}{\mathrm{Re}}\nabla^2 v-a_{0y}, \qquad (2)$$

$$D = \frac{\partial u}{\partial x} + \frac{\partial v}{\partial y} = 0\,, \tag{3}$$

$$\nabla^2 p = 2\left[\frac{\partial u}{\partial x}\frac{\partial v}{\partial y} - \frac{\partial u}{\partial y}\frac{\partial v}{\partial x}\right] - \frac{\partial D}{\partial \mathrm{t}}\,. \tag{4}$$

In these equations ∇^2 is the 2D Laplacian operator, x, y are Cartesian co-ordinates, u, v are the x, y components of velocity in the system fixed to the cylinder, a_{0x}, a_{0y} are the components of cylinder acceleration, p is the pressure and D is dilation. Here Re is the Reynolds number, Re=Ud/ν where d is the cylinder diameter, U is the free stream velocity and ν is the kinematic viscosity.

Although in equation (4) the dilation D = 0 by continuity (3), its partial derivative with respect to time is retained to reduce numerical errors. Equations (1), (2) and (4) will be solved while the continuity equation (3) is satisfied at every time step (see Harlow and Welch, 1965).

No-slip boundary condition is used on the cylinder surface for the velocity and a Neumann-type condition is used for pressure p. Potential flow is assumed far from the cylinder.

Boundary-fitted coordinates are used to impose the boundary conditions accurately. Using unique, single-valued functions, the physical domain bounded by two concentric circles can be mapped into a rectangular computational domain where the spacing is equidistant in both directions. In the physical domain logarithmically spaced radial cells are used, providing a fine grid scale near the cylinder wall and a coarse grid in the far field. Using the mapping functions, not specified here, the governing equations and boundary conditions are transformed into the computational plane. The transformed equations are solved by using the finite difference method. The Poisson equation for pressure is solved by the SOR method. For further details see Baranyi (2003, 2008).

The 2D code developed by the author has been extensively tested against experimental and computational results for a stationary cylinder (Baranyi, 2003, 2008) and computational results for cylinders oscillating in transverse or in in-line directions or following a circular path (Baranyi, 2008), with good agreement being found. For this study the dimensionless time step was 0.0005 and the number of grid points 301x177. For all Re investigated in this study (ranging from Re=120-180) the solution was grid independent. The ratio of the radius of the outer computational domain and cylinder radius was 40.

Figure 1 shows the flow arrangement. The motion of the centre of the cylinder with unit diameter is specified as follows:

$$x_0(t) = A_x\, cos(2\pi f_x t); \quad y_0(t) = -A_y\, sin(2\pi f_y t) \tag{5}$$

where A_x, A_y and f_x, f_y are the dimensionless amplitudes and frequencies of oscillations in x and y directions, respectively. The negative sign in y_0 in equation (5) makes the cylinder orbit clockwise; by changing this sign of y_0 an anticlockwise orbit is obtained. Here f_x=f_y=f, which for nonzero A_x, A_y amplitudes gives an ellipse, shown in the dotted line in Figure 1. A_x with A_y=0 yields pure in-line oscillation, and then as A_y is increased, the ellipticity e=A_y/A_x increases to yield a full circle at e=1. When both amplitudes are zero the cylinder becomes stationary.

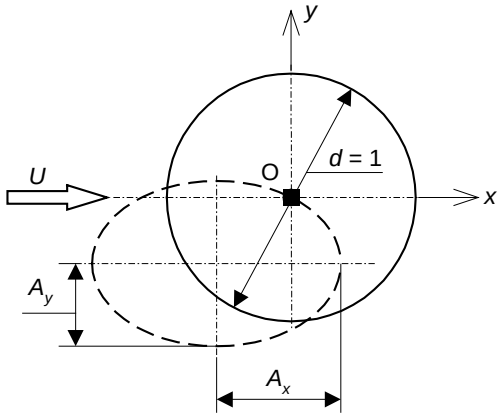

Figure 1: *Layout for the orbital path of the cylinder*

The dimensionless frequency f was kept constant at 85% or 90% of the Strouhal number St_0, i.e., the frequency of vortex shedding from a stationary cylinder at that Reynolds number. Only f=0.9St_0 cases are shown here; results were very similar for both frequencies. These values were chosen because lock-in (synchronisation of frequencies for vortex shedding and cylinder oscillation) was desired without very large amplitudes of A_x and A_y. Only locked-in cases were considered in this study.

3. COMPUTATIONAL RESULTS

3.1 State curves and initial conditions

An interesting phenomenon was observed when looking at the time-mean value (TMV) and root-mean-square (*rms*) values of lift C_L, drag C_D, base pressure coefficients C_{pb}, torque coefficient t_q, and energy transfer E for an orbiting cylinder in a uniform flow. Abrupt jumps were found when these values were plotted against ellipticity e, with Re, A_x and f kept constant (Baranyi, 2004). A typical example for the TMV of lift coefficient for a clockwise orbit is shown in Figure 2 for Re=160,

A_x=0.3, f=0.9St$_0$, St$_0$=0.1882. Note that there are two roughly parallel state or envelope curves. In all computations made so far, C_{Lmean} and t_{qmean} have shown this pattern (subscript *mean* refers to TMV).

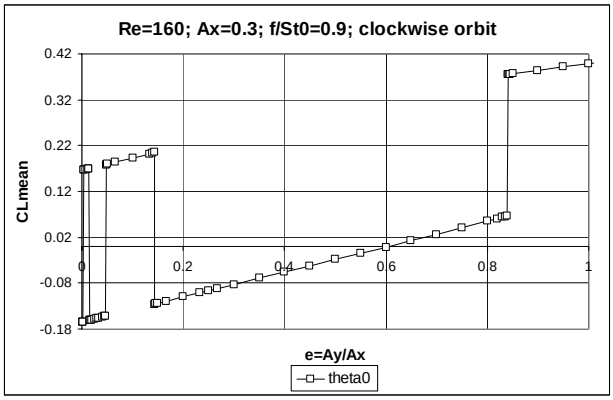

Figure 2: *Time-mean value of lift versus ellipticity*

Figure 3 shows an example of the other state curve pattern, which is found for all *rms* values, for TMV of the drag and base pressure coefficients, and for energy transfer. Here the curves intersect each other at zero ellipticity and then diverge. The location and number of jumps for the curves in Figures 2 and 3 are identical, but the location and number can vary with a change in initial condition Θ (the polar angle characterising the initial cylinder position, from which motion is initiated). The initial condition of Θ=0°, which is the furthest downstream point of the cylinder, was used in the case in Figures 2 and 3. As in all computations shown here, Θ increases in clockwise direction.

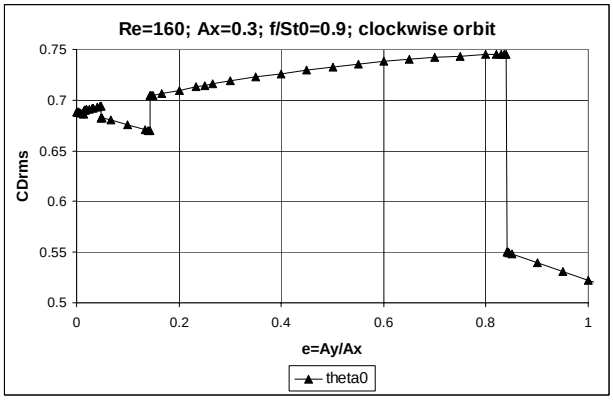

Figure 3: *Rms value of drag versus ellipticity*

The effect of initial condition is demonstrated in Figures 4 and 5, where it can be seen that the full state curves can be reproduced using three different initial conditions (Θ=60°, 90° and 180°). Note that these are for the same set of parameters as in Figures 2 and 3, with the exception of initial condition. The existence of two state curves is clearly seen, showing that two solutions exist, and the solution switches between them (Baranyi 2006, 2008).

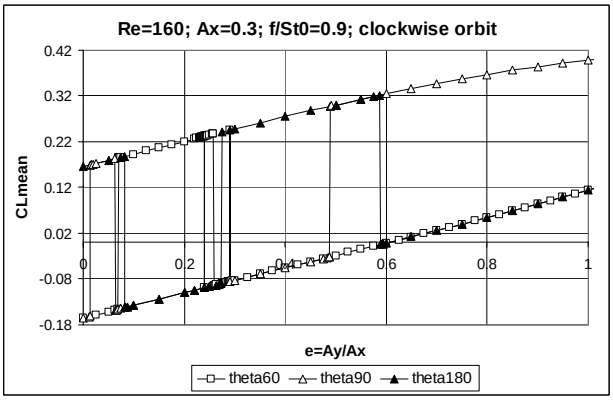

Figure 4: *Time-mean value of lift versus ellipticity: effect of initial condition (Θ=60°, 90° and 180°)*

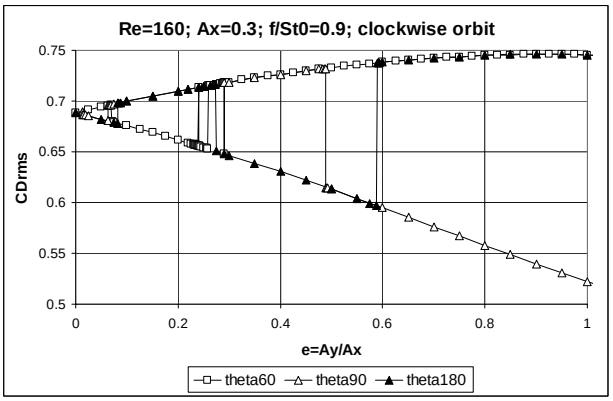

Figure 5: *Rms value of drag versus ellipticity: effect of initial condition (Θ=60°, 90° and 180°)*

3.2 Abrupt alterations in ellipticity

In the cases shown above, each point in the figure was obtained while keeping all five parameters (Re, A_x, e, f/St$_0$, Θ) constant during the course of a single computation. For the following point, ellipticity e was varied by changing A_y. The question arises as to what happens when ellipticity is changed during the course of the computation. This was investigated by altering A_{y1} to A_{y2} abruptly at t_1, to either a larger or smaller value, and continuing the computation long enough to obtain a periodic solution. This is shown in Figure 6, and can also be expressed in mathematical terms as:

if $0 \le t < t_1$ then $A_y=A_{y1}$; if $t_1 \le t \le t_F$ then $A_y=A_{y2}$.

An example for the time history of lift is shown

in Figure 7. The amplitude of transverse oscillation is A_y=A_{y1}=0.0924 until time t_1, when the amplitude is abruptly changed to A_{y2}=0.22. This value is kept constant during the rest of the computation. While there is some transition, the solution becomes periodic soon after the alteration point t_1.

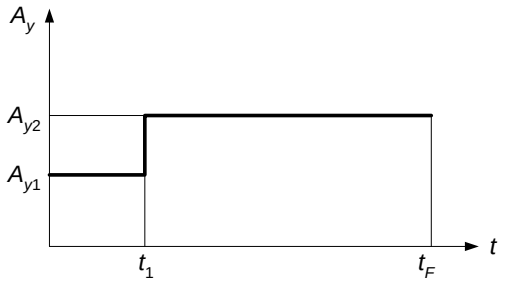

Figure 6: *Layout of transverse amplitude alteration*

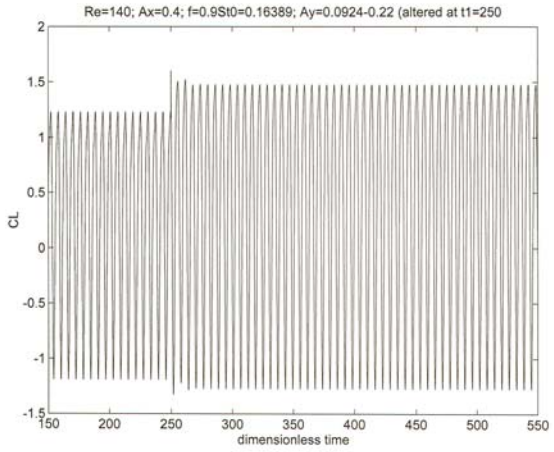

Figure 7: *Time history of lift with amplitude alteration*

The effect of transverse amplitude alteration during the computation is demonstrated in Figures 8-12. While A_{y1} is kept constant for the entire set of computations, A_{y2} is varied for each individual computation. One set of parameters (Re=140; A_x=0.4; f=0.9St$_0$=0.16389) was used in the computations shown in the figures below. If not otherwise stated, Θ=0°. Alteration of A_y took place at t_1=250, and the final dimensionless time t_F=1000, which corresponds to roughly 160 vortex shedding periods. After some transition the solution becomes periodic. After determining the TMV and *rms* values of the periodic signals, each value was plotted at the ellipticity value belonging to A_{y2}. The A_{y1} value for all cases was 0.0924 and the corresponding ellipticity value e_1=0.231. A_{y2} was varied, yielding the filled triangles shown in Figures 8-10.

Figure 8 shows the TMV of lift against ellipticity. The empty squares show results from constant-amplitude computations, and the filled triangles give the results when the amplitude has been abruptly changed during the computation. When the ellipticity is changed from e_1 to e_2, the solution remains in the curve it was in before the alteration, although in the constant-amplitude case, the solution is on the lower curve at that e_2 value. When the difference between e_1 and e_2 becomes large enough, the altered-amplitude solution moves to the other curve (here, at about e=0.84).

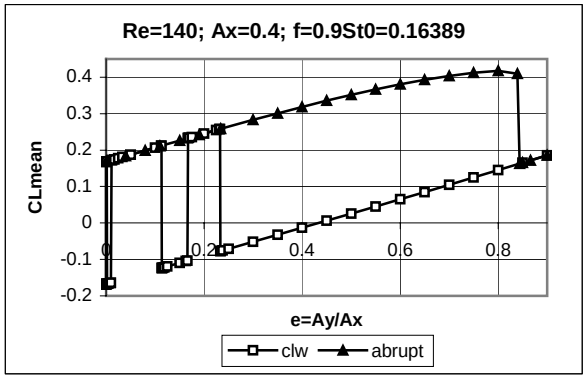

Figure 8: *Time-mean value of lift vs. ellipticity: □ constant amplitude; ▲ abrupt alteration*

Figures 9 and 10 show the TMV and *rms* of the drag coefficient against ellipticity, respectively. Here the values belonging to e_1 are on the lower state curve and the altered-amplitude solutions remain on the lower curve. The solution moves to the other curve at around e=0.84, as for lift, and for all other TMV and *rms* values for this set of data.

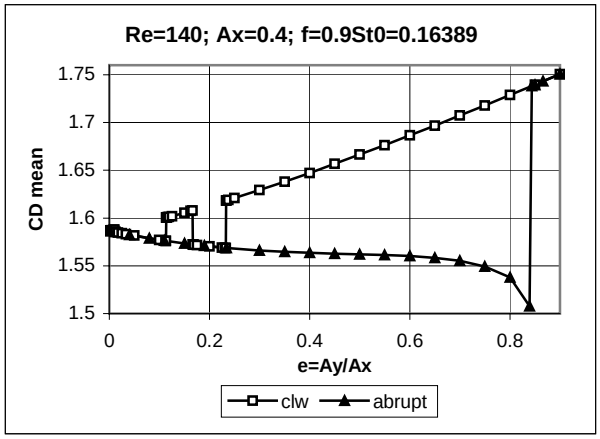

Figure 9: *Time-mean value of drag vs. ellipticity: □ constant amplitude; ▲ abrupt alteration*

It seems that altering the amplitude of oscillation in the course of the computation can keep the force coefficient values in the same curve as before the alteration, thus avoiding (for a certain ellipticity domain) the switch to the other curve. For this particular case, some values (e.g., C_{Lmean} and C_{Lrms}) stay on the upper curve for a longer period, while

others (e.g., C_{Dmean} and C_{Drms}) remain on the lower curve, until approximately e=0.84. After this point, the solution returns to the curve belonging to the constant-amplitude solution (A_y=A_{y1}=A_{y2}).

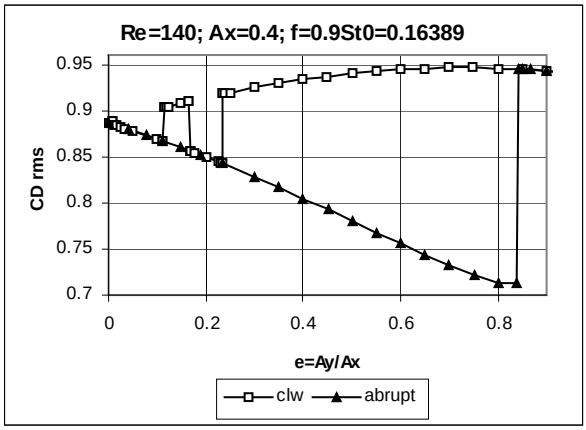

Figure 10: *Rms value of drag vs. ellipticity:* □ *constant amplitude;* ▲ *abrupt alteration*

In discussion of the results shown in Figures 8 and 9, the words 'state curve' were carefully avoided for the curve with the filled triangles, since there was no proof that the curve was a state curve, i.e., the curve belonging to a constant-amplitude solution at that ellipticity value. Repeating constant-amplitude computations under several initial conditions for different ellipticity values can reproduce state curves almost fully (as seen in Figures 4 and 5). It was found that the altered-amplitude results are indeed on the state curve (not shown here for lack of space).

Figure 11 shows three (C_D,C_L) limit cycle curves, two of which coincide with each other. C_D is on the horizontal and C_L is on the vertical axis of the figure. The thick line represents one constant-amplitude case at A_y=0.22 (e=0.55; see Figures 8-10) and Θ=0°. One of the two coinciding thin lines represents the same with Θ=180°, and the other when amplitude was altered during the computation from A_{y1}=0.0924 to A_{y2}=0.22 with Θ=0°. This coincidence of the thin lines and the fact that they differ from the thick line show that (a) altering the amplitude during the computation at the same initial condition (here Θ=0°) results in a very different solution from the constant-amplitude solution; and (b) the altered-amplitude solution is also on a state curve (as it coincides with the constant-amplitude solution at Θ=180°).

Figure 12 displays two coinciding (C_D,C_L) limit cycle curves, one for the constant-amplitude and one for the altered-amplitude case. The parameters are the same as in the case shown in Figure 11 except for A_{y2} which is 0.34 (e=0.85) here. For both curves Θ=0°. Since the ellipticity value here is after the point where the altered-amplitude solution has returned to the same state curve as the constant-amplitude solution, we find that their limit cycle curves are identical, in contrast to the results in Figure 11.

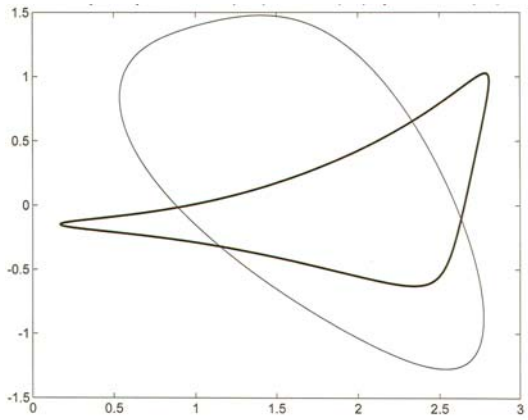

Figure 11: *Three drag-lift limit cycle curves at e=0.55*

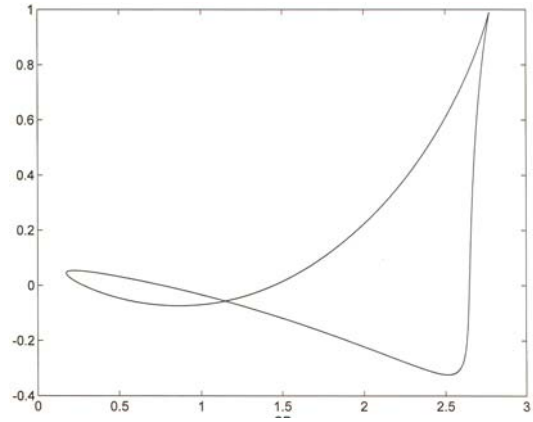

Figure 12: *Two drag-lift limit cycle curves at e=0.85*

4. CONCLUSION

The amplitude of transverse cylinder motion of a cylinder following an orbital path was abruptly altered in the course of computations. These results were compared with solutions obtained when the amplitude was held constant throughout the computation. It was found that:

- an alteration in the amplitude causes the solution to remain on the pre-alteration state curve, at least for some part of the ellipticity domain;
- whether the alteration is an increase or a decrease has no effect on this;
- a substantial alteration in transverse oscillation amplitude is needed in order to shift the solution from its pre-alteration state to the other state.

It seems that the alteration in amplitude works to "conserve the state" and inhibit jumps between states.

Since jumps are inhibited, amplitude alteration could perhaps be used as a means of control to avoid switches in state. Furthermore, in the case shown here, C_L values were kept on the upper state curve and C_D values on the lower for a large part of the ellipticity domain. If this is true of other cases, there may be potential implications for drag reduction.

In order to confirm these findings, investigation of cases with different parameters is necessary. In addition, the effect of altering amplitude gradually rather than abruptly should be investigated.

5. ACKNOWLEDGEMENTS

The support provided by the Hungarian Research Foundation (OTKA, project No. T 068207) is gratefully acknowledged.

6. REFERENCES

Al-Mdallal, Q.M., Lawrence, K.P., Kocabiyik, S., 2007, Forced streamwise oscillations of a circular cylinder: Locked-on modes and resulting fluid forces. *Journal of Fluids and Structures* **23**: 681-701.

Baranyi, L., 2003, Computation of unsteady momentum and heat transfer from a fixed circular cylinder in laminar flow. *Journal of Computational and Applied Mechanics* **4**: 13-25.

Baranyi, L., 2004, Sudden jumps in time-mean values of lift coefficient for a circular cylinder in orbital motion in a uniform flow. In *8th International Conference on Flow-Induced Vibration* (eds E. de Langre & F. Axisa), Paris, Vol. II, 93-98.

Baranyi, L.: Energy transfer between an orbiting cylinder and moving fluid. Paper PVP2006-11-93955. In *ASME Pressure Vessels and Piping Division Conference* (eds J.A. Todd & S.Y. Zamrik), Vancouver, Canada, 2006. on CD ROM.

Baranyi, L., 2007, State curves and flipping for an orbiting cylinder at low Reynolds numbers. In *IUTAM Symposium on Unsteady Separated Flows and Their Control* (eds M. Braza & K. Hourigan), Corfu, Greece, on CD ROM.

Baranyi, L., 2008, Numerical simulation of flow around an orbiting cylinder at different ellipticity values. *Journal of Fluids and Structures* (in press), doi: 10.1016/j.fluidstructs.2007.12.006

Blackburn, H.M., Henderson, R.D., 1999, A study of two-dimensional flow past an oscillating cylinder. Journal of Fluid Mechanics **385**: 255-286.

Blevins, R.D., 1990, *Flow-Induced Vibrations.* Van Nostrand Reinhold, New York.

Didier, E., Borges, A.R.J., 2006, Numerical predictions of low Reynolds number flow over an oscillating circular cylinder. In *Conference on Modelling Fluid Flow* (eds T. Lajos & J. Vad), Vol. I, Budapest, pp. 165-172.

Harlow, F.H., Welch, J.E., 1965, Numerical calculation of time-dependent viscous incompressible flow of fluid with free surface. *Physics of Fluids* **8**: 2182-2189.

Leontini, J.S., Stewart, B.E., Thompson, M.C., Hourigan, K., 2006, Wake state and energy transitions of an oscillating cylinder at low Reynolds number. *Physics of Fluids* **18**: 067101-1-067101-9.

Lu, X.Y., Dalton, C., 1996, Calculation of the timing of vortex formation from an oscillating cylinder. *Journal of Fluids and Structures* **10**: 527-541.

Mureithi, N.W., Rodriguez, M., 2006, Cylinder wake dynamics in the presence of stream-wise harmonic forcing. Paper PVP2006-11-93847. In *ASME Pressure Vessels and Piping Division Conference* (eds J.A. Todd & S.Y. Zamrik), Vancouver, Canada, on CD ROM.

Sarpkaya, T., 1986, Force on a circular cylinder in viscous oscillatory flow at low Keulegan-Carpenter numbers. *Journal of Fluid Mechanics* **165**: 61-71.

Teschauer, I., Schäfer, M., Kempf, A., 2002, Numerical simulation of flow induced by a cylinder orbiting in a large vessel. *Journal of Fluids and Structures* **16**: 435-451.

Williamson, C.H.K., Roshko, A., 1988, Vortex formation in the wake of an oscillating cylinder. *Journal of Fluids and Structures* **2**: 355-381.